IEEE Photonics Journal
An IEEE Photonics Society Publication

A Seven Bit Silicon Optical True Time Delay Line for Ka-Band Phased Array Antenna

Volume 11, Number 4, August 2019

Pengfei Zheng
Chenquan Wang
Xuemeng Xu
Jing Li
Dongdong Lin
Guohua Hu
Ruohu Zhang
Binfeng Yun
Yiping Cui

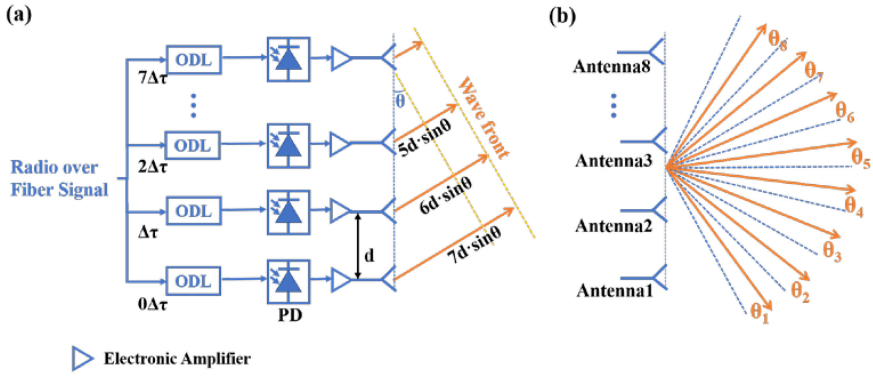

DOI: 10.1109/JPHOT.2019.2927487

A Seven Bit Silicon Optical True Time Delay Line for Ka-Band Phased Array Antenna

Pengfei Zheng, Chenquan Wang, Xuemeng Xu, Jing Li, Dongdong Lin, Guohua Hu, Ruohu Zhang, Binfeng Yun, and Yiping Cui

Advanced Photonics Center, Southeast University, Nanjing 210096, China

DOI:10.1109/JPHOT.2019.2927487

Manuscript received June 6, 2019; revised June 29, 2019; accepted July 5, 2019. Date of publication July 9, 2019; date of current version July 18, 2019. This work was supported in part by the National Key R&D Program of China under Grant 2018YFB2201800, in part by the National Science Foundation of Jiangsu Province under Grant BK 20161429, in part by the National Natural Science Foundation of China under Grant 61601118, and in part by the Postgraduate Research and Practice Innovation Program of Jiangsu Province under Grant KYCX19_0066. Corresponding author: Binfeng Yun (e-mail: ybf@seu.edu.cn).

Abstract: A seven-bit optical true time delay unit with a delay tuning increment of 1.42 ps was designed and fabricated on silicon photonics platform, which can be utilized in Ka-band phased array antenna systems. The delay unit consists of eight thermo-optical switches and seven waveguide delay lines with different lengths. By manipulating the states of the thermo-optical switches, 128 stages of discrete time delays varying from 0 to 191.37 ps has been obtained with low average power consumption of 178.77 mW. Besides, the integrated delay unit was fabricated on the silicon-on-insulator chip that has a very compact footprint of 7.4 mm $\times$ 1.8 mm. In addition, as the waveguide delay dependence on the modulation frequency is very limited and can be neglected, the proposed delay unit should process a large bandwidth that allows it to be utilized in microwave applications with abundant bandwidth.

Index Terms: Microwave photonics, optical true time delay.

1. Introduction

Phased antenna array (PAA) technology was introduced to increasing the communication efficiency via transmitting the microwave signal within a specific direction. By controlling delay times of microwave signals radiating from multiple sub-antennas, the beam pattern of the PAA can be manipulated. Such technology has enormous potential for the wireless communication systems and radar systems [1]. Among the components that forms a PAA, the tunable delay line is the crucial one that determines the performance of the PAA system directly. Recently, microwave photonic delay lines have been widely reported for their low signal loss, broad bandwidth, and immunity to electromagnetic interference compared with their electronic counterparts [2]–[4]. As the surge of integrated microwave photonics, on chip integrated microwave photonics brings new scenario with a reduction in footprint and complexity [5]–[7].

There are several schemes to realize the optical true time delay (OTTD). For non-integrated schemes, there are optical frequency comb combined with dispersion waveguides [8]–[10], two-dimensional array of liquid crystal [11], fiber Bragg gratings [12], etc. For the integrated OTTD,

such as photonic crystal waveguides [13], waveguide Bragg gratings [14], [15], Blass matrix based on optical switches [16], microring resonators (MRR) [17]–[26] and switchable waveguide delay lines [27]–[30] have been demonstrated. Among those schemes, tunable OTTD based MRR and optical switchable waveguides are simple and suitable to be monolithic integrated on silicon on insulator (SOI) chips, therefore, they have attracted increasing interests of the researchers.

In the MRR based OTTD, the optical signals near the resonance wavelength will be delayed due to the resonance effect. And by controlling the coupling coefficient, the group delay can be continuously tuned. However, the delay bandwidth of a single MRR is very limited and there is also a tradeoff between the delay time and the delay bandwidth. Hence, to meet the requirement of broad delay bandwidth, cascaded MRRs based OTTD unit was proposed [17], [18]. The maximum delays of 135 ps and 3.4 ns were achieved in the two works, respectively. However, the delay bandwidths were both smaller than 10 GHz, which would restrict the broadband application. Besides, the introduction of multi-ring structures requires much complex control schemes and higher power consumption. Furthermore, due to the limited bandwidth of MRR, the optical carrier will also be manipulated by the MRR and reduces the OTTD's performance. Therefore, some MRR based OTTD were realized with the optical carrier separated from the sidebands [19]–[21], and resulting in a much more complex control scheme. Besides, MRRs are resonance components whose spectra responses are sensitive to the fabrication variations and thermal variations. Those variations will lead to severe disturbances of the delay and result in the low tuning accuracy of the delay times [22]–[25]. To solve these problems, Choo *et al.* proposed an automatic monitor-based optical beamforming network (OBFN) based on silicon MRRs which operates at 30 GHz with 2 GHz bandwidth [26].

Compared with OTTD based on MRRs, optical switchable waveguide based discrete OTTD has the merits of much wider bandwidth, simple signal processing and controlling, high delay precision and larger tolerance to the fabrication error and thermal variations. Xie *et al.* has reported a seven-bit waveguide delay line based on low loss silicon waveguide, a delay tuning increment of 10 ps was achieved and the maximum delay was larger than 1 ns [28]. Furthermore, they have combined optical switchable waveguide and MRR to realize the continuous delay time tuning [29]. Song *et al.* proposed four-bit reconfigurable true time delay line based on an ultra-low-loss silica waveguide. They have achieved a delay time tuning range from 0 ps to 90.2 ps with an increment of 6 ps [30]. However, the delay tuning increments of aforementioned waveguide based OTTD solutions are about several picoseconds which are not fine enough to meet the requirement of the broadband wireless communication system based on Ka-band PAAs in the future. Due to the increasing of the microwave frequency, the delay increments about 1 ps with sub-picosecond accuracy are required. There are two main challenges that limit the achievement of OTTD with small delay increment. One is the fabrication error that limits the tuning increments, and another challenge is the high-resolution measuring requirement of the delay times. Such OTTD has not been reported to date.

In this paper, we have designed a seven-bit waveguide OTTD unit based on SOI platform that is suitable for a 1×8 Ka-band PAA. The proposed OTTD unit is designed to have a delay increment of 1.42 ps which is the finest to the best of our knowledge. Experiments are carried out to verify the feasibility of the OTTD unit and to characterize its performance. The delay times of the OTTD unit has been experimentally measured by using the optical vector network analysis (OVNA) method based on optical single sideband (OSSB) modulation, and the measuring resolution of 0.1 ps was achieved. The delay time can be discretely tuned from 0 ps through 191.37 ps with an increment of about 1.52 ps in the experimental results. Furthermore, the proposed OTTD unit has a wide bandwidth owing to the wavelength independence of waveguide delay lines.

2. Silicon OTTD Chip Design and Fabrication

As shown in Fig. 1(a), there are eight sub-antennas placed closely adjacent that form a 1×8 PAA. The radiating beam pattern is the interference of the radiations of the eight sub-antennas. The minimum distance between two adjacent sub-antennas should be set as half of the radiated signal's wavelength. For a 40 GHz PAA, the wavelength of the radiated microwave signal is 7.5 mm, hence, the distance d between adjacent sub-antennas should be 3.75 mm. As seen, the radio over fiber

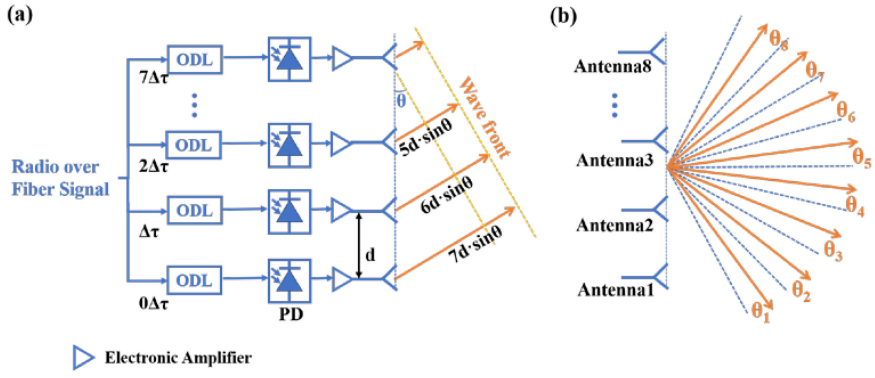

Fig. 1. (a) The schematic diagram of a 1 × 8 phased array antenna based on an optical delay line. (b) The beam radiation directions of the PAA.

signal is separated into eight taps and delayed by eight optical delay lines. Then, the eight taps of optical signals are retrieved by photodetectors. To avoid the power nonuniform of the wavefront, the electronic amplifiers are adopted to balance the RF powers of the eight taps. Then, the RF signals are fed to the eight sub-antennas of the PAA. When there is no time delay between the microwave signal radiated from each sub-antenna, the wave front of the microwave beam will propagate at the angle of $\theta = 0°$.

To change the radiation direction of the beam, phase differences between the antennas should be introduced to change the interference condition and reconstruct the wave front. To eliminate the frequency squint effect, optical true time delay lines are adopted to replace phases shifters, and the beam radiating angle can be modified by controlling the delay time given by:

$$\Delta\tau = \frac{d}{c} \cdot \sin\theta \tag{1}$$

where $\Delta\tau$ is the time delay between adjacent antennas and c is the speed of light in vacuum. In our design, the maximum radiating angle is set as 60°, i.e., the PAA's scanning angle can be manipulated from $-60°$ to 60°. The scanning range is divided into eight parts with an increment about 15° as is illustrated in Fig. 1(b). According to Eq. (1), the increment of the delay time between two adjacent sub-antennas for adjacent scanning angle should be $\Delta\tau = 1.42$ ps.

The required delay time varies from $0\Delta\tau$ to $98\Delta\tau$. A seven-bit OTTD unit can achieve 128 delay time stages which can meet the requirement of the 1 × 8 PAA with eight scanning angles. The OTTD unit is composed of cascaded thermo-optical MZI switches and waveguide delay lines as the structure illustrated in Fig. 2(a). By controlling the states of the switches, different optical paths can be chosen to obtain different optical delay times. Hence, a seven-bit OTTD unit with 128 delay time stages (from $0\Delta\tau$ to $127\Delta\tau$) is designed based on SOI platform as shown in Fig. 2(a). As seen, there are eight thermo-optical MZI switches and seven waveguide delay lines in the OTTD unit. To measure the ON and OFF states of the switches, seven test ports (marked as TP1 to TP7 in Fig. 2(a)) were added to extracted 1% optical power after the switches. Those test ports will introduce an extra insertion loss of 0.3 dB to the OTTD unit. The structure of the thermo-optical MZI switch is shown in Fig. 2(b). Two 2 × 2 multimode interference (MMI) couplers were adopted connected by two 200 μm long strip waveguides. The cross section of the strip waveguide was shown in Fig. 2(c). A TiN heater was fabricated on the modulation arm of the MZI structure. Taking the advantage of the thermo-optical effect of silicon waveguide, the switch can work with a switching power less than 40 mW. As to the waveguide delay line, a low propagating loss is preferred. Here, a ridge waveguide was employed for its low propagation loss compared with strip waveguide. The width of the waveguide is designed as 650 nm and the etching depth is 70 nm with 150 nm remained as the slab as illustrated in Fig. 2(d). The group index of the ridge waveguide is about 3.75478 according to the numerical simulation. Hence, the waveguide lengths of the seven waveguides delay lines are

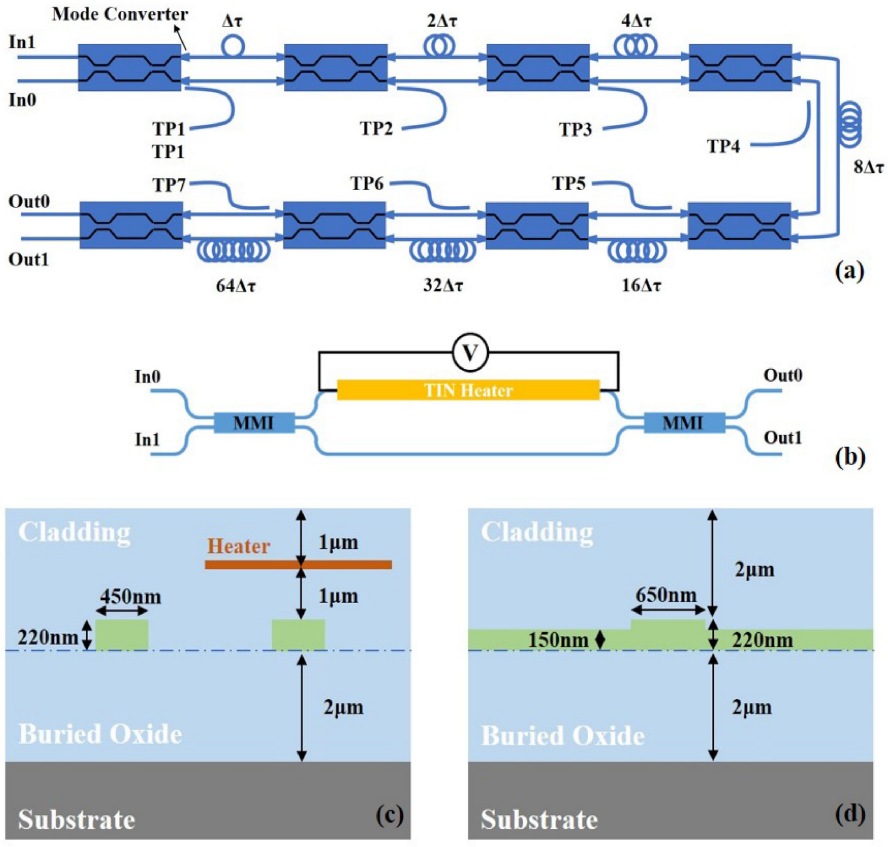

Fig. 2. (a) The architecture of a 7-bit OTTD unit with test ports. (b) The structure of the thermo-optical switch. (c) The waveguide cross section of the thermo-optical switch and (d) the waveguide cross section of the waveguide delay line.

TABLE 1
The Waveguide Lengths of the Seven Ridge Waveguide Delay Lines

Delay time	Δτ	2Δτ	4Δτ	8Δτ	16Δτ	32Δτ	64Δτ
Delay line length (μm)	113.455	226.910	453.821	907.643	1815.286	3630.572	7261.144

calculated and listed in Table 1. Furthermore, the theoretical group velocity dispersion was also simulated. The result shows that with the Ka-band, the dependence of delay time of the OTTD unit is less than 0.01 fs which can be ignored.

The fiber-to-chip and chip-to-fiber coupling of the optical signal were achieved via grating couplers. Moreover, to convert the eigenmode of strip waveguide to the eigenmode of the ridge waveguide adiabatically and vice versa, mode converters with an extremely low insertion loss of 0.02 dB were inserted between the switches and the ridge waveguide delay lines.

The seven-bit OTTD unit was fabricated on a 220 nm SOI wafer. The mask layout of the chip is given in Fig. 3(a). On the 7.8 mm $\times$ 2.85 mm SOI chip, there are a thermo-optical switch, a three-bit OTTD unit and a seven-bit OTTD unit. Fig. 3(b) and 3(c) are the picture of the packaged chip on the designed PCB and the optical microscope image of the fabricated chip, respectively.

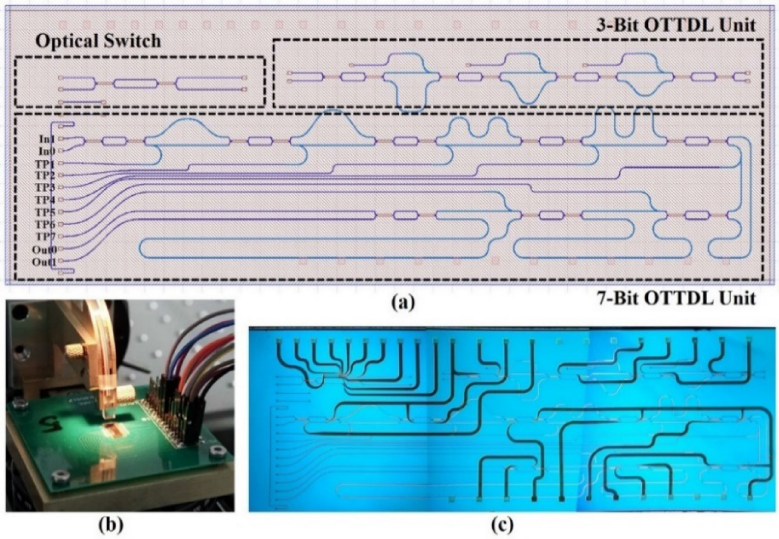

Fig. 3. (a) The mask layout of the designed OTTD unit chip. (b) The packaged chip on the designed PCB. (c) The optical microscope image of the fabricated chip.

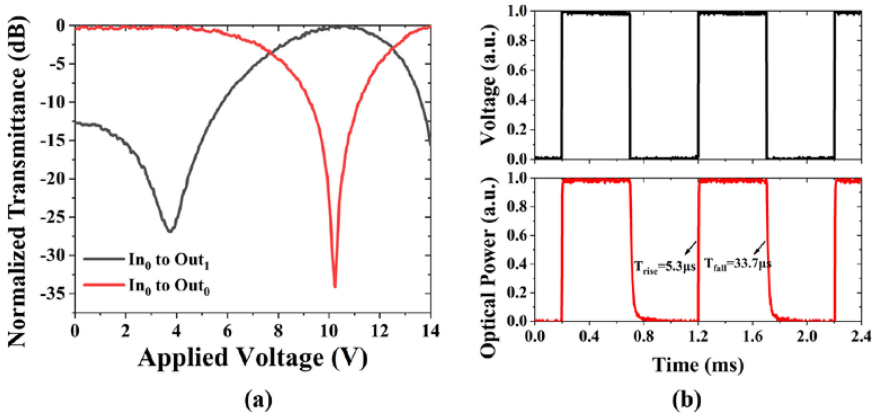

Fig. 4. (a) The switch's transmittances versus the applied voltage tested under "cross" state and "through" state. (b) The transient response of the switch compared with the driving voltage.

3. Measurement Results

First, we have tested the responses of the optical switch under different driving voltage and the transient response. The "cross" state is defined as the optical signal is injected into "in_0" port (or "in_1" port) and then switched to "out_1" port (or "out_0" port). While the "through" state expresses the optical signal travels from "in_0" port (or "in_1" port) to "out_0" port (or "out_1" port). As illustrated in Fig. 4(a), the switch has an extinction ratio larger than 25 dB, which is mainly restricted by the imbalance of the MMI coupler's outputs. The transmittance was normalized to 0 dB and the insertion loss of a single optical switch is about 1.95 dB according to our experimental results. As seen, the "OFF" state voltage and "ON" state voltage of the black curve is about 3.72 V and 10.56 V, respectively. Then, the transient response testing was performed to measure the response time of the optical switch. A square signal with a frequency of 1 kHz was applied to the electrodes of the switch. The lower and higher voltage was set as 3.72 V and 10.56 V, respectively. The rise time and fall time of

TABLE 2
The Resistances, the "Through" and "Cross" State Voltage and the Power Consumption of Each State of the Switches

Switch NO.	Switch1	Switch2	Switch3	Switch4	Switch5	Switch6	Switch7	Switch8
R (kΩ)	6.27	6.963	6.001	6.872	6.241	6.841	7.317	6.494
Vt (V)	10.58	15.58	8.94	14.88	12.01	6.24	8.32	13.02
Vc (V)	14.52	10.92	13.48	10.52	15.46	11.90	13.84	9.06
Pt (mW)	17.85	34.86	13.32	32.22	23.11	5.69	9.46	26.10
Pc (mW)	33.63	17.13	30.28	16.10	38.30	20.70	26.18	12.64

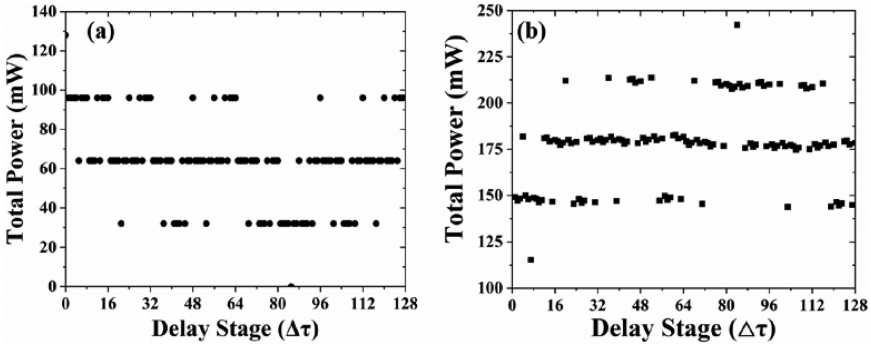

Fig. 5. The total heating power required to obtain the 128 stages of delay times (a) for the theoretical result and (b) for the experimental result.

the switch are 5.3 μs and 33.7 μs, which allow the OTTD unit to switch quickly between different delay time stages as shown in Fig. 4(b).

Then, before measuring the 128 stages of delay times, the "cross" and "through" states of the eight optical switches were measured. To simplify the measurement process, every switch in the OTTD unit was tested only once. The optical signal was injected into the in0 port of the tested switch and the transmittance's dependence on the applied voltage was monitored at the following test port, and a curve that is similar to the curves in Fig. 4(a) was obtained. The voltage of the first minimal transmittance is taken as the "through" state voltage of the switch. Then, the voltage of the adjacent maximal transmittance at the right side of the "through" voltage was taken as the "cross" state voltage of the switch. In this case, we can easily and accurately find out the "through" and "cross" state voltages of the eight optical switches.

The resistances, the applied voltages needed to maintain the "through" states and the "cross" states (denoted as V_t and V_c) and the power consumption (denoted as P_t and P_c) of each state are listed in the following Table 2.

According to Table 2, the switching power of the switches are about 16 mW. If there is no phase differences between the arms of optical switches, the "cross" state power and "through" state power should be 0 and 16 mW, respectively. The average power consumption to realize different delays is, ideally and theoretically, 64 mW. The power consumptions of the 128 delay time stages are illustrated in Fig. 5(a). As seen, the power consumptions are mainly distributed in 5 levels according to their switch states. The smallest power consumption comes from the $85\Delta\tau$ stage ($1\Delta\tau + 4\Delta\tau + 16\Delta\tau + 64\Delta\tau$) and the states of the eight optical switches are all "cross". In the experiment, the "cross" state powers and "through" state powers are different for the eight switches. The measured power needed for the 128 delay stages of the OTTD unit is illustrated in Fig. 5(b). The $83\Delta\tau$ delay requires a switch power of 242.27 mW, which is the maximum among all the 128 delay stages. While the minimum power consumption of 115.27 mW comes from $6\Delta\tau$ delay. The power consumptions of the 128 delay stages also distributed in 5 levels as the switching powers are nearly

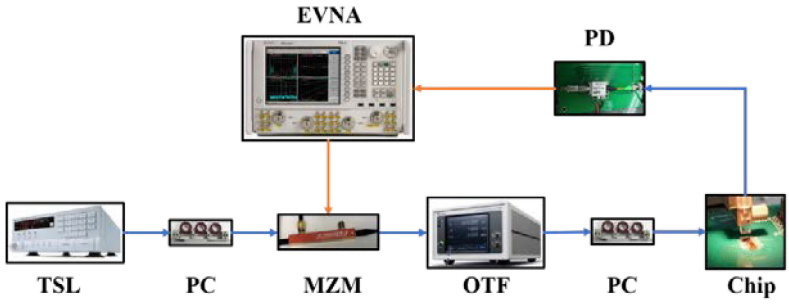

Fig. 6. The experimental setup of the microwave photonics based OVNA link utilized to measure the delay of the OTTD unit. TLS: tunable laser source, PC: polarization controller, MZM: Mach-Zender modulator, OTF: optical tunable filter, PD: photodetector, EVNA: electronics vector network analyzer.

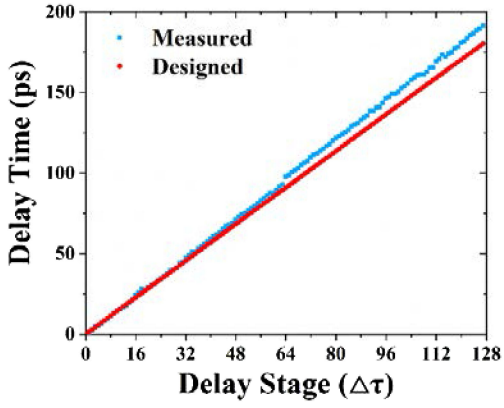

Fig. 7. The measured 128 delay times (from $0\Delta\tau$ to $127\Delta\tau$) compared with the designed delay times.

the same for each optical switch. The measured average power consumption is 178.77 mW which is a little higher than the OTTDs in [28]–[30].

Then, the switchable delay time of the designed seven-bit OTTD unit were measured by utilizing the OVNA method OSSB modulation [31]. Making use of the one-to-one mapping between the optical responses of the optical device and the RF responses of the microwave photonic link, the time delay can be measured accurately with extremely high frequency resolution. To verify the validity of this method, a commercial tunable delay line (General Photonics, VariDelay) was measured with an resolution about 0.1 ps and the measuring results shows great stablility. This allows us to measure the high-resolution delay times of the proposed OTTD unit. The experimental setup was shown in Fig. 6.

In the measurement setup, an optical signal from a tunable laser source (Santac WSL-100), with an output power of 15 dBm, is modulated by a Mach-Zender modulator (EOSpace 10 GHz) working under quadrature bias and generates two optical sidebands. The modulator is driven by the RF signals from the vector network analyzer (Agilent N5242A). Then, the optical signal was fed to an optical tunable filter (Santac OTF-980) to tailor one of the two optical sidebands. A photodetector (Finisar XPDV2120RA), whose responsivity is 0.65 A/W, was adopted to retrieve the RF output signal. Finally, the RF output signal was sent back to the vector network analyzer to obtain the link response. Making use of the one-to-one mapping between the optical phase response and the RF phase response, the phase shift of the OTTD unit can be obtained with an extremely high resolution as well as the optical delays. By controlling the voltages applied on the switches, the 128 stages of delay time can be easily acquired and then measured utilizing the OVNA method.

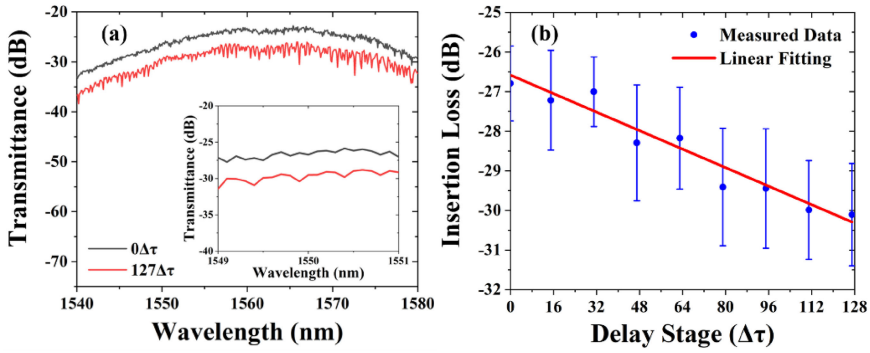

Fig. 8. (a) The spectra of $0\Delta\tau$ delay and $127\Delta\tau$ delay. (b) The insertion losses under different delay stages and their linear fitting.

Fig. 7 shows the measured 128 delay times (from $0\Delta\tau$ to $127\Delta\tau$) compared with the designed values. The measured delay times versus the number of delay stages shows good linearity with a slope about 1.52 ps/stage, which is a bit larger than the designed 1.42 ps/stage. That may result from the fabrication error of the ridge waveguide that leads to the group index deviation between the fabricated chip and the design. When the number of the stage is small, i.e., the optical path is short, the measured delay time matches very well with the designed one, while the deviation increases with the increasing of the optical path.

The spectra of $0\Delta\tau$ delay and $127\Delta\tau$ delay are illustrated in Fig. 8(a). The nonuniform transmittance versus the wavelength is caused by the wavelength dependence of the grating couplers, multimode interference couplers and mode converters. However, the spectra show approximate wavelength independence within a narrow wavelength range from 1549 nm to 1551 nm (corresponding to 250 GHz bandwidth in frequency domain) as illustrated in the inset of Fig. 8(a). When deducting the 11 dB inserting loss of the input and output grating couplers, the on-chip insertion loss of $0\Delta\tau$ delay and $127\Delta\tau$ delay are about 15.64 dB and 19.05 dB, respectively. As shown in Fig. 8(b), we have measured the insertion losses under different delay stages near the wavelength of 1550 nm and the result indicated that the ridge waveguide has a loss of 0.029 dB/stage (2.472 dB/cm). We should also note that the measuring error of the insertion loss is about 3 dB during the experiments owing to power fluctuations caused by the interference of the switches and vibration of the fiber-to-chip coupling platform. The loss of the waveguide delay line can be further reduced by well designing the waveguide bends as is reported in Ref. [32]. Furthermore, the main insertion loss of the OTTD unit comes from the loss of the cascaded optical switches for their simple design and fabrication errors. By redesigning the structure of MMIs and waveguide bends of the optical switch and using low loss fabrication technology [33] in our future works, a much lower insertion loss may be realized.

4. Conclusion

We have demonstrated a seven-bit OTTD unit designed for a 40 GHz PAA. The OTTD unit was fabricated on an SOI chip which has a very compact footprint of 7.4 mm $\times$ 1.8 mm. Eight thermo-optical switches with high switching speed were adopted to control 128 stages discrete delay times varying from 0 ps to 191.37 ps. The average power consumed by the delay stages is 178.77 mW. Also, the waveguide delay line has the natural advantage of insensitivity to wavelength, therefore, the proposed OTTD unit processes a large bandwidth that allows it to be utilized in many broadband microwave applications.

References

[1] H. Hashemi, S. Chu, and J. Roderick, "Integrated true-time-delay-based ultra-wideband array processing," *IEEE Commun. Mag.*, vol. 46, no. 9, pp. 162–172, Sep. 2008.
[2] I. Frigyes and A. J. Seeds, "Optically generated true-time delay in phased-array antennas," *IEEE Trans. Microw. Theory Techn.*, vol. 43, no. 9, pp. 2378–2386, Sep. 1995.
[3] J. Capmany and D. Novak, "Microwave photonics combines two worlds," *Nat. Photon.*, vol. 1, no. 6, pp. 319–330, 2007.
[4] J. Yao, "Microwave photonics," *J. Lightw. Technol.*, vol. 27, no. 3, pp. 314–335, Feb. 2009.
[5] D. Marpaung *et al.*, "Integrated microwave photonics," *Laser Photon. Rev.*, vol. 7, pp. 506–538, 2013.
[6] T. McKenna, J. Nanzer, and T. Clark, "Photonic beamsteering of a millimeter-wave array with 10-Gb/s data transmission," *IEEE Photon. Technol. Lett.*, vol. 26, no. 14, pp. 1407–1410, Jul. 2014.
[7] D. Marpaung, J. Yao, and J. Capmany, "Integrated microwave photonics," *Nat. Photon.*, vol. 13, pp. 80–90, 2019.
[8] X. Ye, F. Zhang, and S. Pan, "Optical true time delay unit for multi-beamforming," *Opt. Exp.*, vol. 23, no. 8, pp. 10002–10008, 2015.
[9] X. Xue, X. Zheng, B. Zhou, and A. Weiner, "Microresonator frequency combs for integrated microwave photonics," *IEEE Photon. Technol. Lett.*, vol. 30, no. 21, pp. 1814–1817, Nov. 2018.
[10] X. Xu *et al.*, "Photonic microwave true time delays for phased array antennas using a 49 GHz FSR integrated optical micro-comb source," *Photon. Res.*, vol. 6, pp. B30–B36, 2018.
[11] X. Yi, T. Huang, and R. Minasian, "Photonic beamforming based on programmable phase shifters with amplitude and phase control," *IEEE Photon. Technol. Lett.*, vol. 23, no.18, pp. 1286–1288, Sep. 2011.
[12] J. Zhang and J. Yao, "Broadband microwave signal processing based on photonic dispersive delay lines," *IEEE Trans. Microw. Theory Techn.*, vol. 65, no. 5, pp. 1891–1903, May 2017.
[13] J. Sancho *et al.*, "Integrable microwave filter based on a photonic crystal delay line," *Nat. Commun.*, vol. 3, 2012, Art. no. 1075.
[14] M. Burla *et al.*, "Integrated waveguide Bragg gratings for microwave photonics signal processing," *Opt. Exp.*, vol. 21, no. 21, pp. 25120–25147, 2013.
[15] J. Wang *et al.*, "Subwavelength grating enabled on-chip ultra-compact optical true time delay line," *Sci. Rep.*, vol. 6, no. 1, 2016, Art. no. 30235.
[16] C. Tsokos *et al.*, "Analysis of a multibeam optical beamforming network based on blass matrix architecture," *J. Lightw. Technol.*, vol. 36, no. 16, pp. 3354–3372, Aug. 2018.
[17] J. Cardenas *et al.*, "Wide-bandwidth continuously tunable optical delay line using silicon microring resonators," *Opt. Exp.*, vol. 18, no. 25, pp. 26525–26534, 2010.
[18] C. Xiang, M. Davenport, J. Khurgin, P. Morton and J. Bowers, "Low-loss continuously tunable optical true time delay based on Si3N4 ring resonators," *IEEE J. Sel. Top. Quant.*, vol. 24, no. 4, 2018, Art. no. 5900109.
[19] L. Zhuang *et al.*, "Single-chip ring resonator-based 1×8 optical beam forming network in CMOS-compatible waveguide technology," *IEEE Photon. Technol. Lett.*, vol. 19, no. 15, pp. 1130–1132, Aug. 2007.
[20] A. Meijerink *et al.*, "Novel ring resonator-based integrated photonic beamformer for broadband phased array receive antennas—Part I: design and performance analysis," *IEEE J. Lightw. Technol.*, vol. 28, no. 1, pp. 3–18, Jan. 2010.
[21] L. Zhuang *et al.*, "Novel ring resonator-based integrated photonic beamformer for broadband phased array receive antennas—Part II: experimental prototype," *J. Lightw. Technol.*, vol. 28, no. 1, pp. 19–31, Jan. 2010.
[22] M. Burla *et al.*, "Integrated photonic Ku-band beamformer chip with continuous amplitude and delay control," *IEEE Photon. Technol. Lett.*, vol. 25, no. 12, pp. 1145–1148, Jun. 2013.
[23] Y. Liu *et al.*, "Tuning optimization of ring resonator delays for integrated optical beam forming networks," *J. Lightw. Technol.*, vol. 35, no. 22, pp. 4954–4960, Nov. 2017.
[24] Y. Liu *et al.*, "Ultra-low-loss silicon nitride optical beamforming network for wideband wireless applications," *IEEE J. Sel. Top. Quant.*, vol. 24, no. 4, Jul./Aug. 2018, Art. no. 8300410.
[25] N. Tessema *et al.*, "A tunable Si3N4 integrated true time delay circuit for optically-controlled K-band radio beamformer in satellite communication," *J. Lightw. Technol.*, vol. 34, no. 20, pp. 4736–4743, Oct. 2016.
[26] G. Choo, C. Madsen, S. Palermo, and K. Entesari, "Automatic monitor-based tuning of an RF silicon photonic 1×4 asymmetric binary tree true-time-delay beamforming network," *J. Lightw. Technol.*, vol. 36, no. 22, pp. 5263–5275, Nov. 2018.
[27] X. Xue *et al.*, "Microcomb-based true-time-delay network for microwave beamforming with arbitrary beam pattern control," *J. Lightw. Technol.*, vol. 36, no. 12, pp. 2312–2321, Jun. 2018.
[28] J. Xie, L. Zhou, Z. Li, J. Wang, and J. Chen, "Seven-bit reconfigurable optical true time delay line based on silicon integration," *Opt. Exp.*, vol. 22, no. 19, pp. 22707–22715, 2014.
[29] X. Wang *et al.*, "Continuously tunable ultra-thin silicon waveguide optical delay line," *Optica*, vol. 4, no. 5, pp. 507–515, 2017.
[30] Q. Song, Z. Hu, and K. Chen, "Scalable and reconfigurable true time delay line based on an ultra-low-loss silica waveguide," *Appl. Opt.*, vol. 57, no. 16, pp. 4434–4439, 2018.
[31] S. Pan and M. Xue, "Ultrahigh-resolution optical vector analysis based on optical single-sideband modulation," *J. Lightw. Technol.*, vol. 35, no. 4, pp. 836–845, Feb. 2017.
[32] M. Cherchi, S. Ylinen, M. Harjanne, M. Kapulainen, and T. Aalto, "Dramatic size reduction of waveguide bends on a micron-scale silicon photonic platform," *Opt. Exp.*, vol. 21, no. 15, pp. 17814–17823, 2013.
[33] M. Moralis-Pegios *et al.*, "On-chip SOI delay line bank for optical buffers and time slot interchangers," *IEEE Photon. Technol. Lett.*, vol. 30, no. 1, pp. 31–34, Jan. 1, 2018.